ARTICLES

Journal of Semiconductors
(2021) 42, 052401
doi: 10.1088/1674-4926/42/5/052401

A complete small-signal HBT model including AC current crowding effect

Jinjing Huang and Jun Liu†

Key Laboratory of RF Circuits and Systems, Ministry of Education, Hangzhou Dianzi University, Hangzhou 310018, China

Abstract: An improved small-signal equivalent circuit of HBT concerning the AC current crowding effect is proposed in this paper. AC current crowding effect is modeled as a parallel RC circuit composed of C_{bi} and R_{bi}, with distributed base-collector junction capacitance also taken into account. The intrinsic portion is taken as a whole and extracted directly from the measured *S*-parameters in the whole frequency range of operation without any special test structures. An HBT device with a 2 × 20 μm^2 emitter-area under three different biases were used to demonstrate the extraction and verify the accuracy of the equivalent circuit.

Key words: small-signal model; HBT; AC current crowding effect

Citation: J J Huang and J Liu, A complete small-signal HBT model including AC current crowding effect[J]. *J. Semicond.*, 2021, 42(5), 052401. http://doi.org/10.1088/1674-4926/42/5/052401

1. Introduction

Heterojunction bipolar transistors (HBTs) have been extensively used in high-speed analog, digital and mixed-signal integrated circuits (ICs)[1–4]. There are several small-signal equivalent circuit topologies for microwave HBT devices' modeling and the accuracy of small-signal model plays a crucial role in the design of ICs.

However, most of the reported topologies ignore the AC current crowding effect[5], which is a critical factor for predicting the AC performance of HBT devices, especially in high frequency range. AC current crowding occurs in the high frequency range related to the bypassing effects of base-emitter capacitance. As the small-signal voltage drops along the intrinsic base region, the diffusion capacitance at the edge of the emitter is proportionally higher than that at the center. This phenomenon can cause the small-signal emitter current to crowd near the edge of the base-emitter junction as frequency increases. Therefore, the intrinsic base capacitance is physically connected with the AC current crowding[6].

In recent years, different small-signal equivalent circuits have been proposed with various extraction methods, in which π[7] or T[8, 9] topologies were used to represent the small-signal equivalent circuits. Heung *et al.*[10] proposed a simple extraction method by using the RC circuit to characterize the AC current crowding effect. However, a simple π-type topology was adopted to extract the intrinsic base capacitance (C_{bi}) through the *Z*-parameter equations. In addition, other papers[11–14] have proposed a more complete small-signal model compared with Ref. [10]. Although their methods have shown good accuracy in the extraction process, more cumbersome analytical methods and calculation cost were needed. Zhang *et al.*[15] proposed a rigorous but concise peeling extraction algorithm. While this method failed to consider the AC current crowding effect, this paper proposes an accurate extraction method with a complete π-type small-signal equivalent circuit considering the AC current crowding effect. This new equivalent-circuit topology is developed based on the small-signal equivalent circuit of an AHBT (agilent heterojunction bipolar transistor) model which has considered the distributed base-collector junction capacitance. Based on the peeling algorithm in Ref. [15] and the T-π transformation presented in Refs. [16–18], a novel method is proposed. In Section 2, an integral small-signal model taking into account the AC current crowding effect is introduced. The parameter extraction procedure is presented in detail in Section 3. Section 4 validates the model performance and a comparison between the proposed model and the conventional model without C_{bi}. Finally, a conclusion is given in Section 5.

2. Small-signal model

The complete small-signal equivalent circuit of the HBT device considering the AC current crowding effect is given in Fig. 1.

In Fig. 1, R_{bx}, R_{cx}, R_e are the base, collector, and emitter parasitic resistances, respectively. R_{bcx} and R_{bex} are the extrinsic base-collector and base-emitter resistances, and C_{bcx} and C_{bex} are the extrinsic base-collector and base-emitter depletion capacitances. R_{bi} and R_{ci} are the intrinsic resistances, and C_{bi} is the intrinsic base capacitance. The parallel RC circuit composed of C_{bi} and R_{bi} characterizes the AC current crowding effect. R_{bci}, R_{bei}, C_{bci} and C_{bei} are the intrinsic resistances and capacitances, respectively. g_m and g_{m0} are the small-signal and DC transconductances, respectively. τ is the delay time.

Circuit topology demonstrated in Fig. 1 can be simplified to facilitate calculation. We introduce three parameters, A_{rbe}, A_{rc} and A_{bex} with a value range of (0, 1) and stipulate $R_{bex} = R_{be}A_{rbe}$, $R_{bei} = R_{be}(1 - A_{rbe})$, $R_{cx} = R_cA_{rc}$, $R_{ci} = R_c(1 - A_{rc})$, $C_{bex} = C_{be}A_{bex}$, and $C_{bei} = C_{be}(1 - A_{bex})$.

Correspondence to: J Liu, ljun77@hdu.edu.cn
Received 27 AUGUST 2020; Revised 8 JANUARY 2021.
©2021 Chinese Institute of Electronics

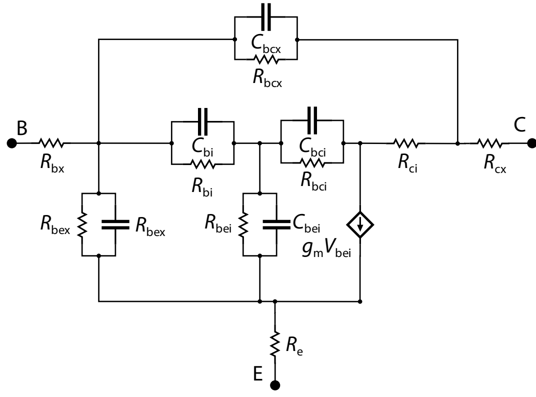

Fig. 1. Complete small-signal equivalent circuit of HBT device including C_{bi}. $g_m = g_{m0}e^{-j\omega\tau}$.

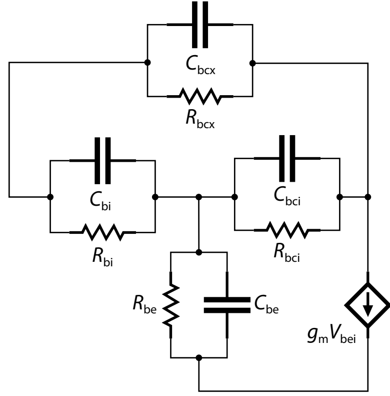

Fig. 2. Small-signal equivalent circuit after de-embedding the extrinsic parameters.

3. Extraction procedure

3.1. Parasitic resistances

Since the parasitic resistances R_{bx}, R_c and R_e are independent of the bias condition, we extract them under zero biasing conditions in this work. The calculation equations are given as follows[19]: $R_{bx} = \text{real}(Z_{11}Z_{12})$, $R_c = \text{real}(Z_{22}Z_{12})$ and $R_e = \text{real}(Z_{12})$. The extracted R_{bx}, R_c and R_e for the 2 × 20 μm^2 HBT device are 6.186, 2.561, and 5.526 Ω, respectively. The impedance matrix Z_m after de-embedding R_{bx}, R_c and R_e from the total two-port Z-parameters Z can be written as

$$[Z_m] = Z - \begin{bmatrix} R_{bx}+R_e & R_e \\ R_e & R_c+R_e \end{bmatrix}. \quad (1)$$

Through Y–Z transformation, Y_m can also be expressed as

$$Y_{m11} = \frac{Z_{be}+Z_{bci}}{N} + Y_{bcx}, \quad (2)$$

$$Y_{m12} = \frac{-Z_{be}}{N} - Y_{bcx}, \quad (3)$$

$$Y_{m21} = \frac{g_m Z_{be} Z_{bci} - Z_{be}}{N} - Y_{bcx}, \quad (4)$$

$$Y_{m22} = \frac{Z_{be}+Z_{bi}(1+g_m Z_{be})}{N} + Y_{bcx}, \quad (5)$$

where $Z_{be} = R_{be}/(1+j\omega R_{be}C_{be})$, $Z_{bci} = R_{bci}/(1+j\omega R_{bci}C_{bci})$, $Z_{bi} = R_{bi}/(1+j\omega R_{bi}C_{bi})$, $Y_{bcx} = 1/R_{bcx} + j\omega C_{bcx}$, $N = Z_{bi}Z_{be} + Z_{bi}Z_{bci} + Z_{be}Z_{bci}$.

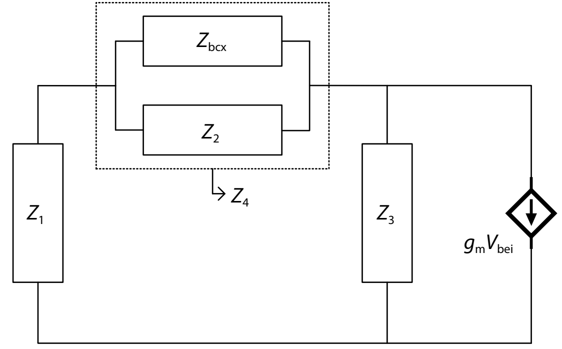

Fig. 3. Final circuit after T-π transformation.

3.2. Intrinsic part parameters

Once the parasitic resistances are known, the extraction of the intrinsic parameters can be carried out[20]. The circuit is presented in Fig. 2, and the admittance parameter of the intrinsic part Y_{in} can be written as

$$[Y_{in}] = [Y_m] - \begin{bmatrix} 0 & 0 \\ 0 & Y_o \end{bmatrix}. \quad (6)$$

The circuit in Fig. 2 can be converted to that in Fig. 3 after T-π transformation[21] with $Z_4 = Z_2Z_{bcx}/(Z_2+Z_{bcx})$. The parameters Z_1, Z_2, and Z_3 can be derived from Eq. (6) as follows

$$Z_1 = \frac{N}{Z_{bci}}, \quad (7)$$

$$Z_2 = \frac{N}{Z_{be}}, \quad (8)$$

$$Z_3 = \frac{N}{Z_{bi}}. \quad (9)$$

Combining Eqs. (6)–(9), Y_{in} can also be represented by Z_1, Z_2, Z_3, and Z_4, which are expressed as[16]

$$[Y_{in}] = \begin{bmatrix} \frac{1}{Z_1}+\frac{1}{Z_4} & -\frac{1}{Z_4} \\ X\frac{Z_3}{Z_1}-\frac{1}{Z_4} & \frac{1}{Z_3}+\frac{1}{Z_4}+X \end{bmatrix}, \quad (10)$$

in which

$$X = Bg_m, \quad (11)$$

$$B = \frac{Z_1}{Z_1+Z_2+Z_3}. \quad (12)$$

Then, we can get that

$$Z_1 = \frac{1}{Y_{in11}+Y_{in12}}, \quad (13)$$

$$Z_3 = \frac{Y_{in11}+Y_{in21}}{(Y_{in11}+Y_{in12})(Y_{in22}+Y_{in12})}, \quad (14)$$

$$Z_4 = -\frac{1}{Y_{in12}}. \quad (15)$$

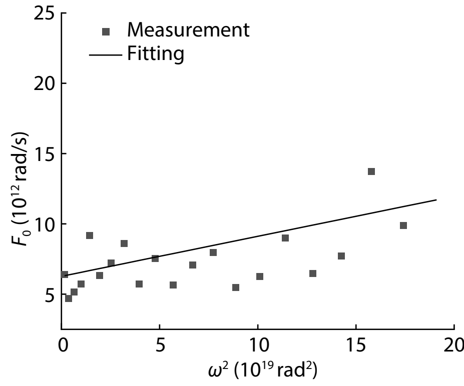

Fig. 4. Frequency of F_0 versus ω^2.

Based on the above relationship between Y_{in} and Z_1, Z_2, Z_3, the extraction method reported in Ref. [18] is used to extract the parameters. From Eqs. (13) and (14), we can get

$$\frac{Z_1}{Z_3} = \frac{R_{bi}}{R_{bci}} \frac{1 + j\omega R_{bci} C_{bci}}{1 + j\omega R_{bi} C_{bi}}, \tag{16}$$

$$\mathrm{real}\left(\frac{Z_1}{Z_3}(1 + j\omega T_{bi})\right) = \frac{R_{bi}}{R_{bci}}, \tag{17}$$

$$\mathrm{imag}\left(\frac{Z_1}{Z_3}(1 + j\omega T_{bi})\right) = \omega R_{bi} C_{bci}. \tag{18}$$

Defining

$$T_{bi} = R_{bi} C_{bi},$$
$$F_0 = \frac{\omega}{\mathrm{imag}\left(\frac{Z_1}{Z_3}\right)} = A_0 + \omega^2 B_0, \tag{19}$$

where $A_0 = 1/\alpha_0$, $B_0 = T_{bi}^2/\alpha_0$, $\alpha_0 = R_{bi}(R_{bci} C_{bci} - T_{bi})/R_{bci}$.

Since Z_1 and Z_3 are given in Eqs. (13) and (14), the ω^2 dependence of F_0 can be easily plotted in Fig. 4. Then A_0 and B_0 can be determined. T_{bi} is defined as

$$T_{bi} = \sqrt{\frac{B_0}{A_0}}. \tag{20}$$

Based on Eq. (7), Z_1 can be written as

$$Z_1 = \frac{R_{bi}}{1 + j\omega T_{bi}} + \frac{R_{be}}{1 + j\omega T_{be}} + \frac{R_{bi}}{1 + j\omega T_{bi}} \frac{R_{be}}{1 + j\omega T_{be}} \frac{1 + j\omega T_{bci}}{R_{bci}}, \tag{21}$$

$$Z_1(1 + j\omega T_{bi}) = \frac{R_x(1 + j\omega T_x)}{1 + j\omega T_{be}}, \tag{22}$$

where

$$R_x = R_{bi} R_{be}\left(\frac{1}{R_{bci}} + \frac{1}{R_{be}} + \frac{1}{R_{bi}}\right), \tag{23}$$

$$T_x = \frac{C_{bci} + C_{be} + C_{bi}}{\frac{1}{R_{bci}} + \frac{1}{R_{be}} + \frac{1}{R_{bi}}}, \tag{24}$$

$$T_{be} = R_{be} C_{be}, \tag{25}$$

$$T_{bci} = R_{bci} C_{bci}. \tag{26}$$

Defining

$$F_1 = \frac{\omega}{\mathrm{imag}(Z_1(1 + j\omega T_{bi}))} = A_1 + \omega^2 B_1, \tag{27}$$

where $A_1 = 1/\alpha_1$, $B_1 = T_{be}^2/\alpha_1$, $\alpha_1 = R_x(T_x - T_{be})$.

A_1 and B_1 can be obtained by using the straight-line fitting method. Then, T_{be} can be determined as

$$T_{be} = \sqrt{\frac{B_1}{A_1}}. \tag{28}$$

Based on Eqs. (22) and (25), we can get

$$F_2 = Z_1(1 + j\omega T_{bi})(1 + j\omega T_{be}) = R_x(1 + j\omega T_x). \tag{29}$$

By extracting the real and imaginary parts of F_2, R_x and T_x can be acquired from Eqs. (30) and (31).

$$\mathrm{real}(F_2) = R_x, \tag{30}$$

$$\mathrm{imag}(F_2) = \omega R_x T_x. \tag{31}$$

Based on Eqs. (23) and (24), the expressions of R_x and $R_x T_x$ can be written as

$$R_x = \left(1 + \frac{R_{bi}}{R_{bci}}\right) R_{be} + R_{bi}, \tag{32}$$

$$R_x T_x = (T_{bi} + R_{bi} C_{bci}) R_{be} + T_{be} R_{bi}. \tag{33}$$

R_{be}, R_{bi} can be determined from Eqs. (17), (18), (20), (28), (30), and (31). When R_{be} and R_{bi} are obtained, R_{bc}, C_{bc}, C_{be} and C_{bi} can be obtained from Eqs. (17), (18), (25), and (26), respectively.

In the end, the remaining parameters are written as $C_{bcx} = \mathrm{imag}(1/Z_4 - 1/Z_2)/\omega$, $R_{bcx} = \mathrm{real}(1/Z_4 - 1/Z_2)^{-1}$. g_{m0} and τ are obtained from Eqs. (11) and (12): $g_{m0} = |X/B|$ and $\tau = -\mathrm{phase}(X/B/g_{m0})/\omega$.

4. Model verification

An GaAs HBT with 2 μm emitter linewidth was used to validate the accuracy of the equivalent circuit. The adopted device was manufactured in a commercial foundry. The method in Section 3 is applied to extract the parameters of an HBT device with a 2 × 20 μm² emitter-area under bias points of Bias1 (V_{ce} = 1 V, I_b = 15 μA), Bias2 (V_{ce} = 1 V, I_b = 30 μA) and Bias3 (V_{ce} = 3 V, I_b = 17.5 μA) in the frequency range from 100 MHz to 20 GHz. After extracting all parameters, the Keysight ICCAP software is used to optimize the extracted parameters to further reduce the error between the simulated and measured data. Here, the initial values of A_{rbe}, A_{rc} and A_{bex} are set to 0.5 for optimization. Results of the extraction are compared with the extracted from the small-signal equivalent circuit of an AHBT (agilent heterojunction bipolar transistor) without considering C_{bi}. Table 1 shows the initial extraction and optimization results of the HBT device under Bias1 and Bias3. The comparisons of the real part and the imagin-

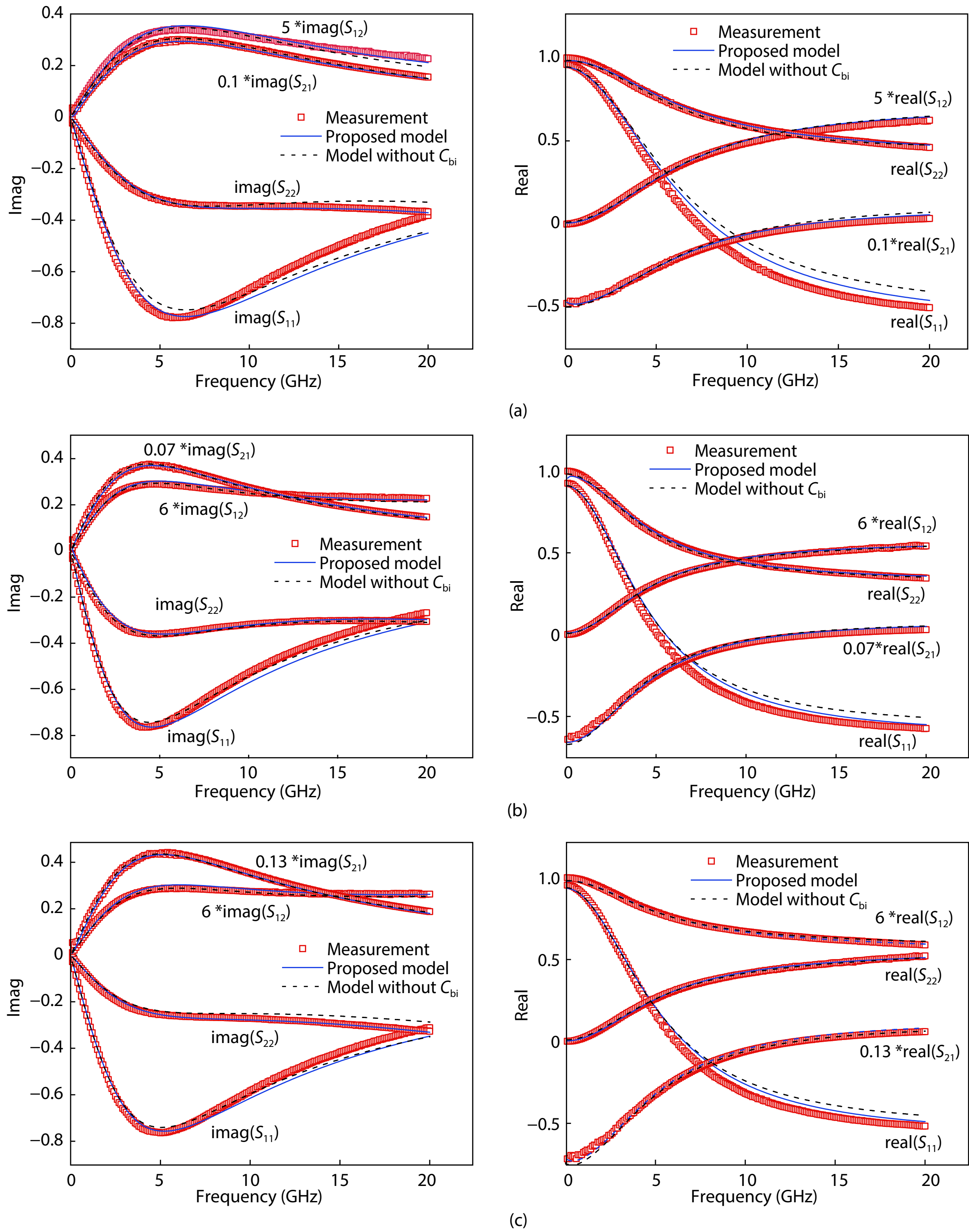

Fig. 5. S-parameters comparisons in the frequency range from 100 MHz to 20 GHz under the biasing condition: (a) Bias1 (V_{ce} = 1 V, I_b = 15 μA), (b) Bias2 (V_{ce} = 1 V, I_b = 30 μA), (c) Bias3 (V_{ce} = 3 V, I_b = 17.5 μA).

ary part between the simulated and measured S-parameters are plotted in Fig. 5. The accuracy of S-parameters versus frequency shows in Table 2.

Due to the inaccurate initial value of 0.5 for the partition parameters A_{rc}, A_{rbe}, and A_{bex} defined before extraction, the extracted and optimized values of R_{cx}, R_{ci}, R_{bcx}, R_{bex}, C_{bcx} and C_{bex} are slightly larger. From Fig. 6, it can be seen that the proposed model with C_{bi} shows more accuracy than the one without C_{bi}, which verifies the effectiveness of the introduced AC current crowding effect.

Fig. 6 shows the decrease of C_{bi} with I_b and V_{ce}. Results present that C_{bi} decreases with increasing I_b and V_{ce}, which is consistent with the result shown in Ref. [18]. The experimental results show that the dependence between C_{bi} and biases accords with the basic capacitance equation.

5. Conclusion

An improved small-signal equivalent circuit of the HBT device considering the AC current crowding effect is proposed in this paper. This effect is modeled as a parallel RC circuit with C_{bi} and R_{bi}. By comparing between the simulated and measured S-parameters under three different biases, the

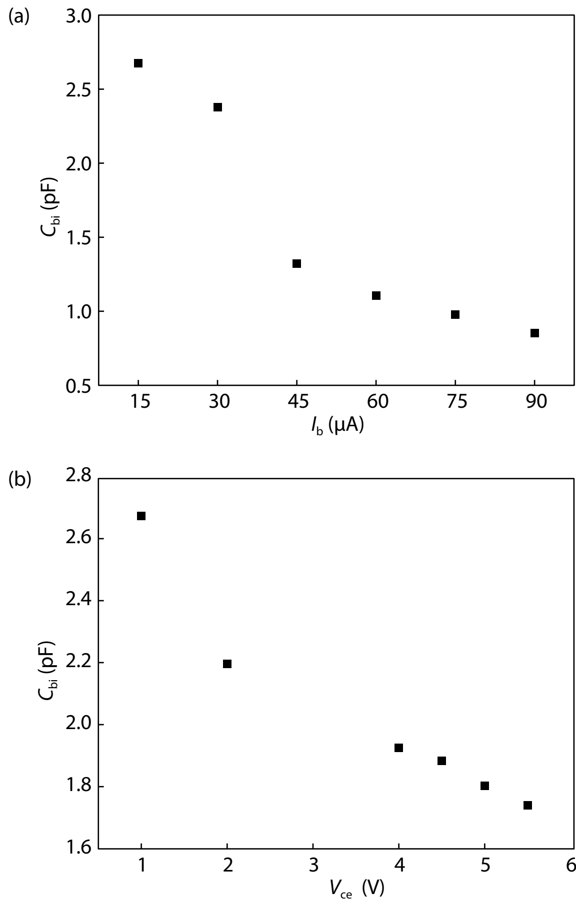

Fig. 6. (a) Plot of C_{bi} versus I_b. (b) Plot of C_{bi} versus V_{ce}.

results validate the reliability and availability of the proposed model and the developed extraction method.

Acknowledgements

This work was supported by the National Natural Science Foundation of China (Grant No. 61934006)

References

[1] Zhang J, Liu M, Wang J, et al. Modeling of InP HBTs with an improved keysight HBT model. Microw J, 2019, 62(7), 56

[2] Shivan T, Weimann N, Hossain M, et al. A highly efficient ultrawideband traveling-wave amplifier in InP DHBT technology. IEEE Microw Wirel Compon Lett, 2018, 28(11), 1029

[3] Griffith Z, Urteaga M, Rowell P. A 190-GHz high-gain, 3-dBm OP1dB low DC-power amplifier in 250-nm InP HBT. IEEE Microw Wirel Compon Lett, 2017, 27(12), 1128

[4] Lin Q, Wu H, Chen Y J, et al. A 0.5 to 4.0 GHz low-cost broadband GaAs HBT low noise amplifier. 2019 IEEE MTT-S International Wireless Symposium (IWS), 2019

[5] Huang S C, Tang W B, Hsin Y M. High-frequency noise modeling of InGaP/GaAs HBT with base-contact capacitance and AC current crowding effect. IEEE Electron Device Lett, 2009, 30(11), 1125

[6] Yadav S, Chakravorty A, Schroter M. Modeling of the lateral emitter-current crowding effect in SiGe HBTs. IEEE Trans Electron Devices, 2016, 63(11), 4160

[7] Yapei C, Yong Z, Yuehang X, et al. Investigation of terahertz 3D EM simulation on device modeling and a new InP HBT dispersive inter-electrode impedance extraction method. IEEE Access, 2018, 6, 45772

[8] Gloria, Daniel, Danneville, et al. Small-signal characterization and modelling of 55 nm SiGe BiCMOS HBT up to 325 GHz. Solid State

Table 1. The initial extraction and optimization results of the HBT under Bias1 (V_{ce} = 1 V, I_b = 15 μA) and Bias3 (V_{ce} = 3 V, I_b = 17.5 μA). Error = |Extracted – Optimized| / Extracted × 100%.

Parameter		Extracted	Optimized	Error (%)
R_{bx} (Ω)	Bias1	6.897	7.723	11.98
	Bias3	6.897	8.65	25.42
R_{cx} (Ω)	Bias1	1.281	1.591	24.20
	Bias3	1.281	1.271	0.781
R_{ci} (Ω)	Bias1	1.281	0.970	24.28
	Bias3	1.281	0.961	24.98
R_e (Ω)	Bias1	6.526	5.289	18.95
	Bias3	6.526	8.417	28.98
R_{bcx} (kΩ)	Bias1	239.9	246.1	2.584
	Bias3	571.6	569.3	0.402
C_{bcx} (fF)	Bias1	34.92	34.82	0.286
	Bias3	30.32	28.58	5.739
R_{bex} (kΩ)	Bias1	2.093	5.500	162.8
	Bias3	1.590	2.621	64.84
C_{bex} (fF)	Bias1	208.5	127.6	38.80
	Bias3	639.5	208.6	67.38
R_{bi} (Ω)	Bias1	306.7	309.0	0.750
	Bias3	627.9	541.4	13.78
C_{bi} (pF)	Bias1	2.058	2.033	1.215
	Bias3	1.271	1.203	5.350
R_{bci} (kΩ)	Bias1	140.4	139.1	0.926
	Bias3	271.5	296.8	9.319
C_{bci} (fF)	Bias1	1.764	1.773	0.510
	Bias3	1.069	1.088	1.777
R_{bei} (Ω)	Bias1	2.093	1.490	28.81
	Bias3	1.590	0.553	65.22
C_{bei} (fF)	Bias1	208.5	289.9	39.04
	Bias3	639.5	1,049	64.03
R_o (kΩ)	Bias1	12.54	12.84	2.390
	Bias3	6.666	5.244	21.33
C_o (fF)	Bias1	23.48	20.43	12.99
	Bias3	17.61	17.63	0.114
g_{m0} (mS)	Bias1	79.77	80.03	0.326
	Bias3	227.5	227.9	0.176
τ (ps)	Bias1	2.317	2.821	21.75
	Bias3	2.834	3.179	12.17

Table 2. The accuracy of *S*-parameters versus frequency.

Bias	*S*-parameter	Without C_{bi} (%)	With C_{bi} (%)
Bias1	S11	85.13	89.31
	S12	91.78	94.65
	S21	88.37	92.63
	S22	97.06	98.39
Bias2	S11	91.62	91.68
	S12	95.06	95.86
	S21	92.35	93.44
	S22	97.70	98.21
Bias3	S11	91.16	92.51
	S12	93.49	96.71
	S21	93.17	93.82
	S22	96.38	99.12

Electron, 2017, 129, 150

[9] Sun Y, Fu J, Wang Y, et al. Direct analytical parameter extraction for SiGe HBTs T-topology small-signal equivalent circuit. Superlattices Microstruct, 2016, 94, 223

[10] Rhee H S, Lee S, Kim B R. D. c. and a. c. current crowding effects model analysis in bipolar junction transistors using a new extraction method. Solid-State Electron, 1995, 38(1), 31
[11] Tang W B, Wang C M, Hsin Y M. A new extraction technique for the complete small-signal equivalent-circuit model of InGaP/GaAs HBT including base contact impedance and AC current crowding effect. IEEE Trans Microw Theory Tech, 2006, 54, 3641
[12] Lee K, Choi K, Kook S H, et al. Direct parameter extraction of SiGe-HBTs for the VBIC bipolar compact model. IEEE Trans Electron Devices, 2005, 52(3), 375
[13] Dousset D, Issaoun A, Ghannouchi F M, et al. Wideband closed-form expressions for direct extraction of HBT small-signal parameters for all amplifier bias classes. IEEE Proceedings - Circuits, Devices and Systems, 2005, 152(5), 441
[14] Johansen T K, Leblanc R, Poulain J, et al. Direct extraction of InP/GaAsSb/InP DHBT equivalent-circuit elements from S-parameters measured at cut-off and normal bias conditions. IEEE Trans Microw Theory Tech, 2016, 64(1), 115
[15] Zhang J C, Liu B, Zhang L M, et al. A rigorous peeling algorithm for diret parameter extraction procedure of HBT small-signal equivalent circuit. Analog Integr Circuits Signal Process, 2015, 85(3), 405
[16] Bousnina S, Mandeville P, Kouki A B, et al. Direct parameter-extraction method for HBT small-signal model. IEEE Trans Microw Theory Tech, 2002, 50(2), 529
[17] Degachi L, Ghannouchi F M. Systematic and rigorous extraction method of HBT small-signal model parameters. IEEE Trans Microw Theory Tech, 2006, 54(2), 682
[18] Degachi L, Ghannouchi F M. An augmented small-signal HBT model with its analytical based parameter extraction technique. IEEE Trans Electron Devices, 2008, 55(4), 968
[19] Zhou W, Sun L, Liu J, et al. Extraction and verification of the small-signal model for InP DHBTs in the 0.2–325 GHz frequency range. ICE Electron Express, 2018, 15(13), 20180244
[20] Zhang A, Gao J, Wang H. Direct parameter extraction method for InP heterojunction bipolar transistors based on the combination of T- and π-models up to 110 GHz. Semicond Sci Technol, 2019, 35(2), 025001
[21] Zhang A, Gao J. A direct extraction method to determine the extrinsic resistances for InP HBT device based on S-parameters measurement up to 110 GHz. Semicond Sci Technol, 2020, 35(7), 075025

Jinjing Huang is a MS student in Key Laboratory of RF Circuits and Systems in Hangzhou Dianzi University. She obtained her BS from Hangzhou Dianzi University in 2018. She focuses on the modeling of semiconductor devices.

Jun Liu received his master's degree from Hangzhou Dianzi University in 2006 and his doctor's degree from Dublin City University in 2011. He is now a professor at the School of Electronic Information, Hangzhou Dianzi University. His main research interest includes device equivalent circuit modeling, RF/MMIC design, CAD/EDA tool development.